Nonlinear ion transport mediated by induced charge in ultrathin nanoporous membranes

J. Pedro de Souza,[1,*] Chun-Man Chow,[1,*] Rohit Karnik,[2] and Martin Z. Bazant[1,3]

[1]*Department of Chemical Engineering, Massachusetts Institute of Technology, 25 Ames St., Cambridge, Massachusetts 02142, USA*

[2]*Department of Mechanical Engineering, Massachusetts Institute of Technology, 77 Massachusetts Ave., Cambridge, Massachusetts 02139, USA*

[3]*Department of Mathematics, Massachusetts Institute of Technology, 182 Memorial Drive, Cambridge, Massachusetts 02142, USA*

(Received 13 July 2021; accepted 7 September 2021; published 26 October 2021)

Ultrathin membranes with nanoporous conduits show promise for ionic separations and desalination applications, but the mechanisms underlying the nonlinear ionic transport observed in these systems are not well understood. Here, we demonstrate how induced charge at membrane interfaces can lead to nonlinear ionic transport and voltage-dependent conductance through such channels. The application of an electric field on a polarizable membrane leads to induced charges at the membrane interfaces. The induced charges in turn are screened by diffuse charges in the electrolyte, which are acted upon by the electric field. For extremely thin membranes, the induced charge effect can be significant even for moderate applied voltages commonly used in experiments. We apply a continuum Poisson-Nernst-Planck model to characterize the current-voltage behavior of ultrathin membranes over a wide parameter space. The predictions of the model are compared to recent experiments on graphene and MoS_2 membranes in an electric field. We expect the role of induced charge to be especially pronounced in the limit of atomically thin membranes.

DOI: 10.1103/PhysRevE.104.044802

I. INTRODUCTION

Recent advances in synthesis and fabrication techniques enable the creation of well-defined nanopores in two-dimensional (2D) materials such as graphene and MoS_2, which allows for the control of mass transport on the molecular level [1]. These nanoporous atomically thin membranes show molecular selectivity between gas species, salt ions, and dye molecules while allowing for high fluxes due to their extreme thinness, which, together with their demonstrated high mechanical strength and chemical robustness, makes them promising for a wide range of applications [2–6]. These include CO_2 capture, natural gas purification, solvent/petrochemical separations, desalination, dialysis, DNA sequencing, and energy harvesting [7–12].

Despite such development, the fundamental transport mechanisms across the nanopores have not been fully understood. The last decade has seen an increase in studies attempting to understand the transport of molecules and ions through these nanopores using both experimental and simulation techniques. One of the most commonly performed experiments to understand ion transport involves measuring the current (I) of ions under an applied electric potential (V), and determining the conductance (G) of the nanopore using these I-V curves using the relationship $I = GV$. Molecular dynamics and continuum Poisson-Nernst-Planck (PNP) simulations have been used to explain the experimental results [12–16]. Most of these studies focus on the linear portion of the I-V curve, where the conductance is constant, even though many experimental I-V curves across different systems (over a wide range of pore sizes and different materials) have significant nonlinear characteristics. The nonlinearity is often only briefly discussed, and is attributed to the surface charge on the nanopore or the breakdown of the ion's hydration shell at high voltages that is difficult to test [13,14]. These previous discussions have overlooked an effect quite common in the electrokinetics literature—the induced charge (IC) effect—that could help explain the nonlinearity and provide a scaling model for the I-V relationship.

Induced charge effects have been widely studied as an electrokinetic phenomenon especially in microfluidic systems, where miniaturization is associated with favorable scaling [17,18]. These include induced-charge electro-osmosis (ICEO), where flow is created by an applied electric field acting on free charge induced by the field itself on double layers on the surface of polarizable objects [19–21], and induced-charge electrophoresis, where a polarizable object moves by an electric field acting upon the induced double layers [22–24]. These have various applications in microfluidic mixing and pumping, electrical actuation and sensing, and controlling electrolysis and electrodeposition [25–27]. The IC effect also influences the transport characteristics of membranes with micro- and nanoscale pores. Notably, electric fields near the corners of polarizable membranes and conduits lead to ICEO vortices that affect corner deposition of colloids and microfluidic mixing [28–30]. Mao *et al.* noted the IC effect in their continuum simulations of nanochannels in a thin silica membrane, but focused primarily on the fluid flow field rather than the I-V characteristics [31]. Further, the role of induced charges has been investigated in terms of membrane stability [32,33] and for conduction through conical nanopores [34]. Based on these previous studies, the IC effect appears especially relevant for membranes in the atomically thin limit.

[*]These authors contributed equally to this work.

For polarizable membranes, which includes graphene and MoS_2, an externally imposed electric potential difference would induce charge displacement in the membrane as it polarizes in response to the electric field. Oppositely charged counterions accumulate in the solution adjacent to the membrane surfaces, leading to higher ionic charge densities and thus higher conductivities around the membrane pore, irrespective of the fluid flow. The nonlinearity of the *I-V* curves could then stem from the voltage-enhanced conductance due to the IC effect.

Ultrathin membranes, especially atomically thin ones such as graphene and MoS_2, exhibit high capacitance because capacitance scales inversely with membrane thickness, which in turn is expected to lead to more pronounced induced charge effect compared to thicker membranes. Although their measured and calculated permittivities could vary across studies, typical values are in the range of $\epsilon_m \sim 3\epsilon_0$ for MoS_2 and $\sim 6\epsilon_0$ for graphene, and would also depend on the pore/defect density and chemical doping [35–38]. This leads to per area capacitance on the order of $C_m \sim 10^0 - 10^1\ \mu\mathrm{F/cm^2}$.

Researchers have shown that surface charges affect 2D membrane transport properties and can impart selectivity between different ions or molecules [13,15,39–41]. Instead of grafting charged chemical moieties at the pores, one can also modulate surface charge by connecting an electrode to a conductive or semiconductive membrane, and control the charge by changing the applied voltage [42]. However, with IC, even without direct electrode connection to the membrane, a potential gradient and surface charge can be induced across the membrane via an external electric field, as in many of the experimental setups studying *I-V* relationships. The ability to modulate charges without the need for direct electrode conduction or creating charged functional groups at the pores would enable more functionalities and flexibility in device design. Furthermore, it might allow for biomimetic voltage-dependent ion conductance and selectivity reminiscent of selective biological ion channels [43].

Here we construct a continuum model to describe the induced charge effect in ultrathin nanoporous membranes. We also offer a simple scaling model for quick predictions. We compare the model predictions to previously published experimental results, and discuss extensions of the model.

II. METHODS

To investigate the induced charge phenomenon, we consider a steady current through a nanopore in a thin film (membrane) driven by a voltage difference. Standard PNP equations were used in the electrolyte solution domains. We also consider the Poisson equation within the membrane itself, which is often neglected in PNP simulations that only set a fixed surface charge boundary condition. Here we neglect fixed surface charge to focus exclusively on the induced charge effect. Table I summarizes the key simulation parameters implemented for a 1:1 electrolyte solution. This validation data set allows for characterization of the induced charge effect as a function of ionic concentration, pore radius, membrane thickness, membrane permittivity, and applied voltage. Additional parameters are also tested in direct comparison to experimental results depending on the identity of the electrolyte ionic solution, the membrane, and the pore domain.

TABLE I. Simulation validation set parameters. Bolded values are used as the "base case" for Fig. 2.

Type	Symbol	Value(s)	Units	Description
Ion	c_0	1, 10, 100[a]	mM	Bulk concentration
	D	2×10^{-9}	$\mathrm{m^2\ s^{-1}}$	Diffusivity
	z	±1		Valence
Membrane	R	0.2, 0.5, **1**	nm	Pore radius
	L	**0.5**, 0.65, 1	nm	Thickness
	ϵ_m/ϵ_0	3, **6**, 20		Permittivity
Simulation	V	0.01 −1	V	Applied voltage
	ϵ_w/ϵ_0	80		Solution permittivity
	T	298	K	Temperature
	W	240	nm	Reservoir width (radius)
	H	240	nm	Reservoir height

[a]The Debye lengths corresponding to $c_0 = 1, 10, 100$ mM for $z = 1$ are $\lambda_D = 9.7, 3, 0.97$ nm, respectively.

The simulations are composed of an electrolyte domain Ω_w and a membrane domain Ω_m, as shown in Fig. 1. A cylindrical pore of radius R connects the two electrolyte reservoirs of equal ionic concentration through a membrane of thickness L. In the electrolyte domain, the steady state ion concentration profiles are solved assuming Nernst-Planck fluxes, j_i,

$$\nabla \cdot \mathbf{j_i} = 0, \quad \mathbf{j_i} = -D_i \nabla c_i - \frac{D_i z_i F c_i}{R_g T} \nabla \phi. \tag{1}$$

Here, c_i is the concentration, z_i is the valency, and D_i is the diffusivity of species i. ϕ is the electrostatic potential, F is Faraday's constant, R_g is the ideal gas constant, and T is the temperature. In the electrolyte domain, the electrostatic potential satisfies Poisson's equation with charge density ρ_e:

$$-\epsilon_w \nabla^2 \phi = \rho_e \tag{2}$$

assuming a constant bulk permittivity of water $\epsilon_w = 80\epsilon_0$. In the membrane domain, we assume that the ion concentration is zero and that the membrane acts as an ideal dielectric, in which Laplace's equation is satisfied for the electrostatic potential:

$$\nabla^2 \phi = 0. \tag{3}$$

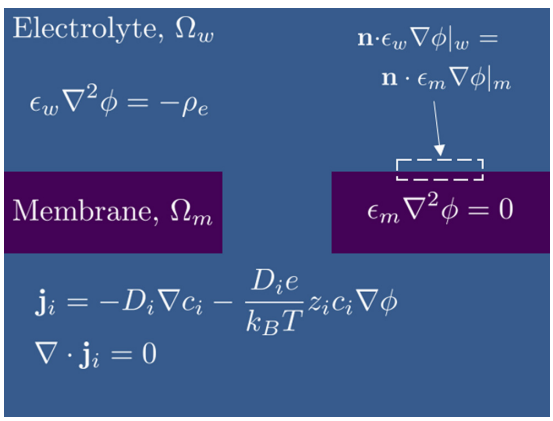

FIG. 1. Simulation setup for the nanopore system using an axisymmetric geometry.

At the membrane boundaries, in the absence of fixed surface charges, the electric field satisfies

$$\mathbf{n} \cdot \epsilon_w \nabla \phi|_w = \mathbf{n} \cdot \epsilon_m \nabla \phi|_m. \tag{4}$$

where ϵ_m is the membrane permittivity. This boundary condition allows the normal electric field to enter the membrane domain. Many models neglect the electric field in the membrane domain, but we show that, for sufficiently thin membranes, the normal electric field induces charge at the membrane interfaces even at moderate applied voltages. The action of the applied voltage on the diffuse double layers screening the induced membrane charge leads to nonlinear current-voltage characteristics.

We implement the system of equations in the finite-element solver COMSOL MULTIPHYSICS using the General Form PDE interface. The cylindrical pore is centered about $r = 0$ in the axisymmetric simulation domain, and the pore openings corresponding to the membrane thickness are set at $z = 0$ and $z = L$. On either side of the membrane, there are reservoirs of height H, and the simulation domain is enclosed by a cylindrical boundary. At $r = W$, the reservoir radius, a zero flux boundary condition is imposed for ionic concentrations and normal electric field. At the top and bottom of the electrolyte domain, at $z = L + H$ and $z = -H$, Dirichlet boundary conditions are imposed specifying the ionic concentration and potential at the boundary. The values of W and H were chosen to be sufficiently large so as to not affect the ionic concentration and potential profiles near the pore, even at low ionic concentrations. We restrict our analysis to the case where the two sides of the membrane are held at the same concentration, as commonly applied in experimental measurements.

While the continuum approach proposed here may have significant errors at the molecular scale, such models are routinely applied to describe ionic conduction and selectivity in the nanoscale regime. Certainly, additional contributions to the ionic chemical potential from ionic finite size, specific ionic chemical character, and electrostatic correlations may impact the microscopic physics of induced charge formation at the pore entrance [44]. Ionic paring and ionic reactions could also affect the ionic profiles and transport characteristics. The image charge effects of ions near the membrane interfaces, dielectric saturation of solvent molecules, and dielectric decrement in response to ionic concentration variations are not included in the model. Furthermore, we neglect the coupled Stefan-Maxwell diffusion of ions and the coupling between ion transport and fluid flow, since we are principally concerned with ionic conduction. Even so, the continuum approach allows us to define a baseline prediction that can be compared to experimental results to quantify the extent of induced charge on the conductance of pores in atomically thin membranes.

III. RESULTS AND DISCUSSION

Our results of the simulation are presented as follows. First, we discuss the general characteristics of the simulation results including the I-V curves predicted by the model, as well as the ionic concentration and potential distributions in the presence of induced membrane charge. Next, we apply the model to understand the expected extent of induced charge effects in experimental observations of activated nonlinear currents through atomically thin membranes. Finally, we derive approximate formulas that can capture the trends in the induced charge effect as a function of the simulation parameters from (1) simple scaling arguments and (2) a more detailed analytical transport model.

A. Simulation features

The simulation reproduced the nonlinear, activated I-V characteristics observed in many experimental studies at higher voltages, a subset of which is shown in Fig. 2. All of them deviate from the typical linear current-voltage behavior: $I = GV$ with constant $G = G_0$, suggesting the presence of additional voltage effects which could be explained by the IC phenomenon on the membrane. Larger pores lead to higher currents by decreasing both access resistance (i.e., that faced by the ions as they converge from bulk into the nanopore restriction) and channel resistance (i.e., across the pore itself) [45], whereas thinner membrane and higher membrane permittivity are associated with higher membrane capacitance that leads to higher induced charge effects and thus larger currents. The IC effect is stronger at lower concentrations (larger Debye lengths), as indicated by the higher relative current scaled by the bulk ion concentration. The induced charge has a more drastic effect on the local ionic conductivity relative to the bulk conductivity at lower concentrations.

The cross sections of the pore in Fig. 3 illustrate the elevated ionic density at the membrane interfaces and in the pore domain as a function of applied voltage for a set of sample parameters. At low applied voltage, the ionic concentrations are more or less constant. However, at high applied voltages, the ions accumulate more intensely due to the IC effect, with positive (negative) ions concentrated on the top (bottom) side of the membrane where the relative potential is greater (lower) to screen the induced surface charge on the membrane, leading to higher solution conductivity around the pore. The concentration profile of each ion is perturbed drastically by the presence of the pore, where the screening charges on each interface are swept through the pore and enriched at the pore exit on the opposite side of the membrane. As the double layer thickness is comparable to the pore size for the parameters tested, the ionic enrichment within the pore spans the pore diameter for thin membranes with small pores.

Figure 4 displays how the potential decays for low and high applied voltages. Normalized to the applied voltage, the potential decays more slowly for the pore with more induced charge at higher applied voltage. In both systems, the potential decays as $1/r$ far from the pore, as plotted in Fig. 4(c). Evidently, the pore with induced charge exhibits a larger effective electrical pore size, as signaled by the expanded contours in the electrostatic potential far from the pore. At high applied voltage, the double layers on each interface provide a low resistance pathway to deliver additional current to the pore mouth, and higher ionic concentration within the pore itself translates to lower resistance within the pore. These effects combined create a voltage-dependent conductance through the pore domain, and thus nonlinear current-voltage relationships.

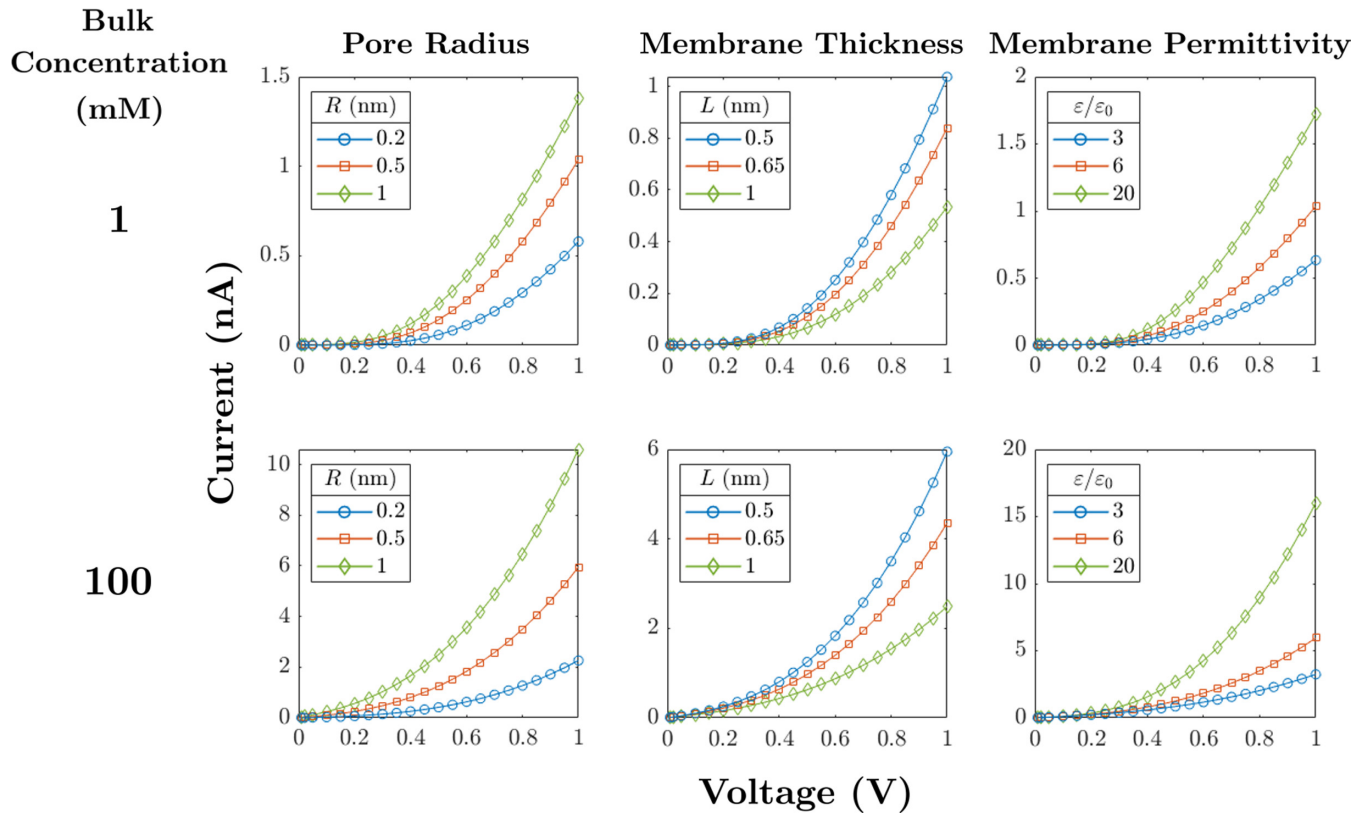

FIG. 2. Current-voltage (I-V) curves for a subset of simulations for various pore radii (left), membrane thicknesses (center), and membrane permittivities (right), holding other values at their base case (Table I). The simulation data points were connected with straight lines to guide the eye. The top and bottom rows correspond to a bulk salt concentration of 1 and 100 mM, respectively.

B. Comparison with experimental observations

We also demonstrate that the induced charge phenomenon could be used to explain the nonlinear I-V curve behaviors observed in experiments. Figures 5 and 6 compare the simulation results to experimental electrical measurements in nanopores in the chemical vapor deposition graphene of Jain *et al.* with inherent defects and the focused (gallium) ion beam irradiated MoS_2 of Thiruraman *et al.* [13,14]. In order to make the comparison, the radius of the pore, R, is fitted to reproduce the conductance at low voltages near zero applied voltage (where induced charge is not present). Then, all parameters are kept constant as the voltage is varied. The diffusivities of each ion everywhere in the electrolyte domain is assumed to be equal to the diffusivity in the bulk [13]. For lower salt concentrations ($\approx$100 mM), a graphene permittivity of 7, which is on the order of literature reported value, is able to reproduce the nonlinear observations that yield close predictions of the current for monovalent (LiCl and KCl) and divalent salts ($MgCl_2$, $CaCl_2$, and $BaCl_2$), as shown in Fig. 5.

However, at higher concentrations ($\approx$1 M), the induced charge effect cannot account for the full extent of nonlinearity in the I-V relationships using the same fixed values of the membrane permittivity for graphene and MoS_2, as shown in Fig. 6. It is possible that the electronic properties of the membrane, especially in the presence of large ionic concentrations near the pore, might lead to an effective membrane permittivity or capacitance that is higher than the expected value. For the nonlinearity at high ionic concentration to be entirely attributable to the IC effect, the effective permittivity of the membrane would need to be higher than the fixed parameters we have chosen. To quantify the required permittivity, we also varied the membrane permittivity to qualitatively match the shape of the nonlinearities for the conductance measured at high concentration. For the graphene pore, a relative permittivity of $\sim$40 is needed, while for MoS_2, a relative permittivity of $\sim$20 is needed. These curves are included in Fig. 6 to indicate the extent of rectification for larger effective membrane permittivities. The effective permittivity values may inflate the membrane capacitance unrealistically, since they are much larger than the literature values for graphene and MoS_2. Evidently, even the large value of permittivity of graphene cannot capture the full rectification at negative voltages observed for the experimental sample. In such situations, it is evident that other mechanisms such as ionic dehydration may play a role alongside the induced charge effect.

Another note must be made that the induced charge effect as presented in our model can only capture the "activated" curves, where the conductance magnitude only increases with increasing applied voltage magnitude. More complex nonlinearities like rectification and deactivation either require some (i) breaking of symmetry in the membrane domain or (ii) high voltage inhibitive effect like the crowding of ions [44]. We restrict our analysis and comparisons only to the activation of the ionic currents at high voltage due to the known limitations of our model.

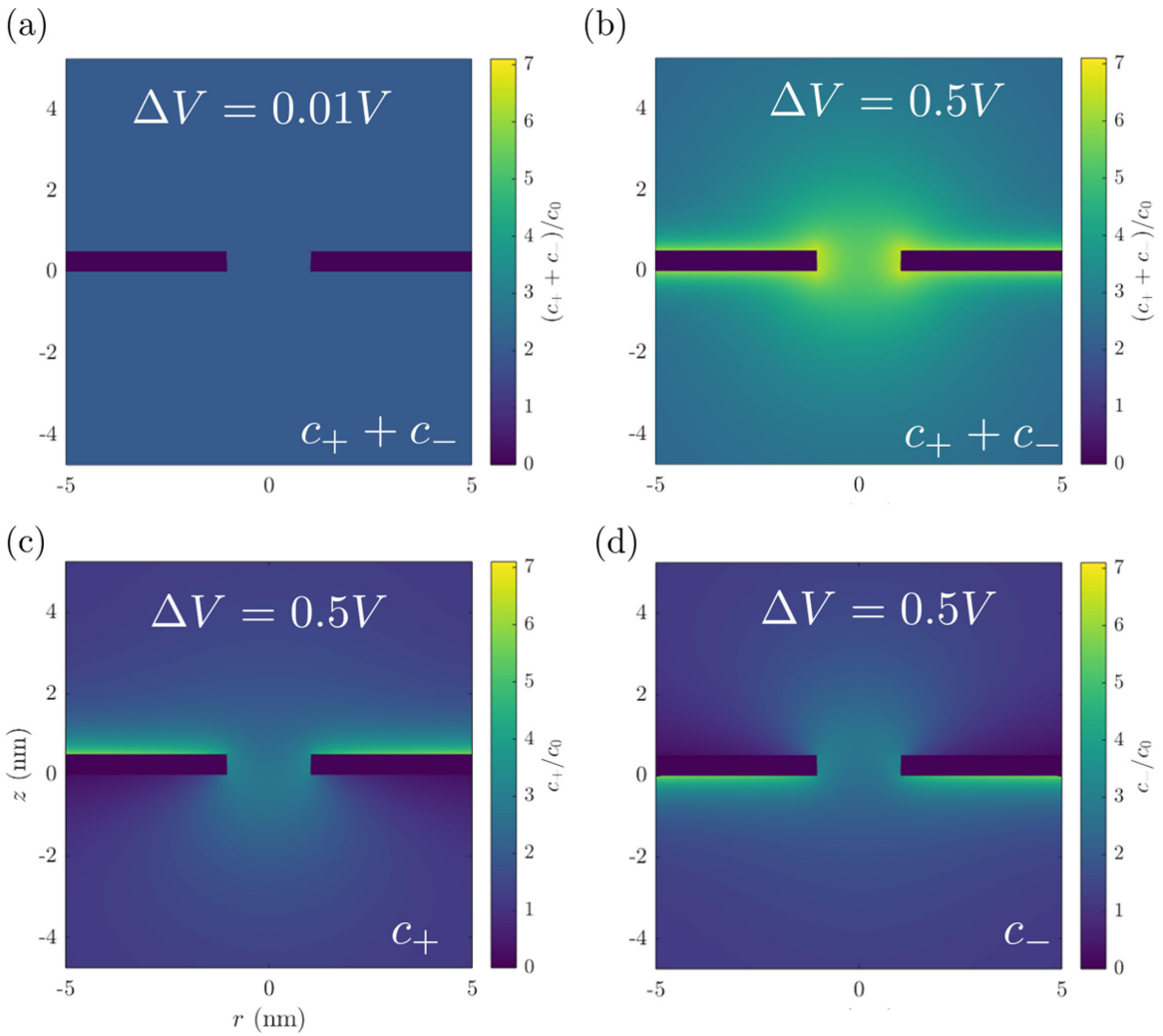

FIG. 3. Total ion density around the pore at (a) low ($\Delta V = 0.01$ V) and (b) high ($\Delta V = 0.5$ V) applied voltage for $c_0 = 100$ mM, $R = 1.0$ nm, $L = 0.5$ nm, $\epsilon_m = 6\epsilon_0$. (c) Cation and (d) anion concentration profiles corresponding to (b) at $\Delta V = 0.5$ V. The ionic densities are normalized by the bulk salt concentration in the reservoir.

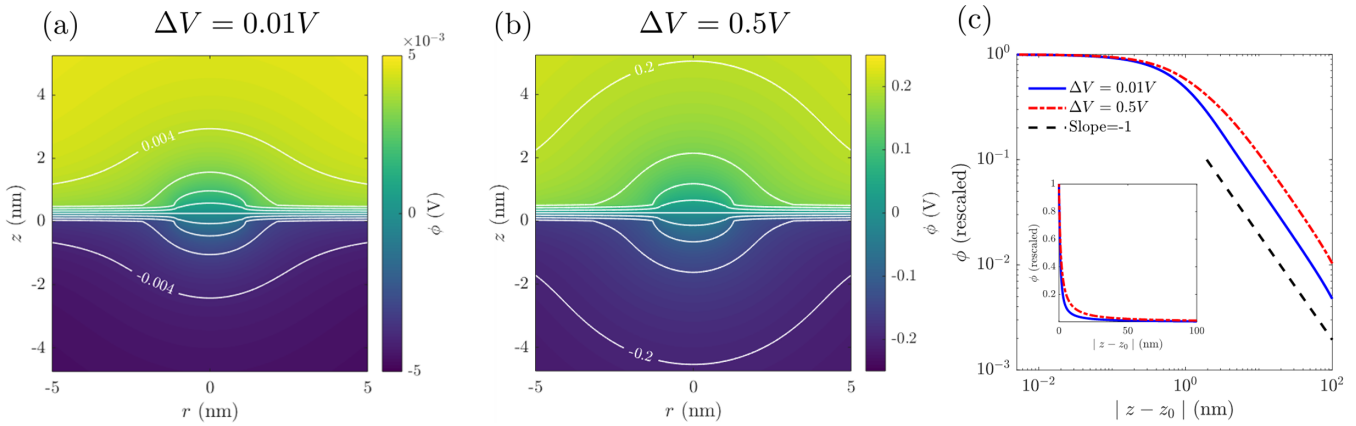

FIG. 4. Electrostatic potential around the pore at (a) low ($\Delta V = 0.01$ V) and (b) high ($\Delta V = 0.5$ V) applied voltage for $c_0 = 100$ mM, $R = 1$ nm, $L = 0.5$ nm, $\epsilon_m = 6\epsilon_0$. Equally spaced contours of the potential are shown in white. The outer contours corresponding to 80% of the ΔV are labeled as $\pm 0.004\ V$ and $\pm 0.2\ V$. (c) The potential from the center of the pore entrance along the negative z axis of the simulation domain for both low and high applied voltages, where $z_0 = 0$ is the opening of the pore mouth. The potential is rescaled such that its value is zero at $z \to -\infty$, and then the value of the potential is rescaled by its value at the pore entrance at $r = 0$ and $z = 0$. The potential decay is plotted on a log-log scale (main) and linear-linear scale (inset).

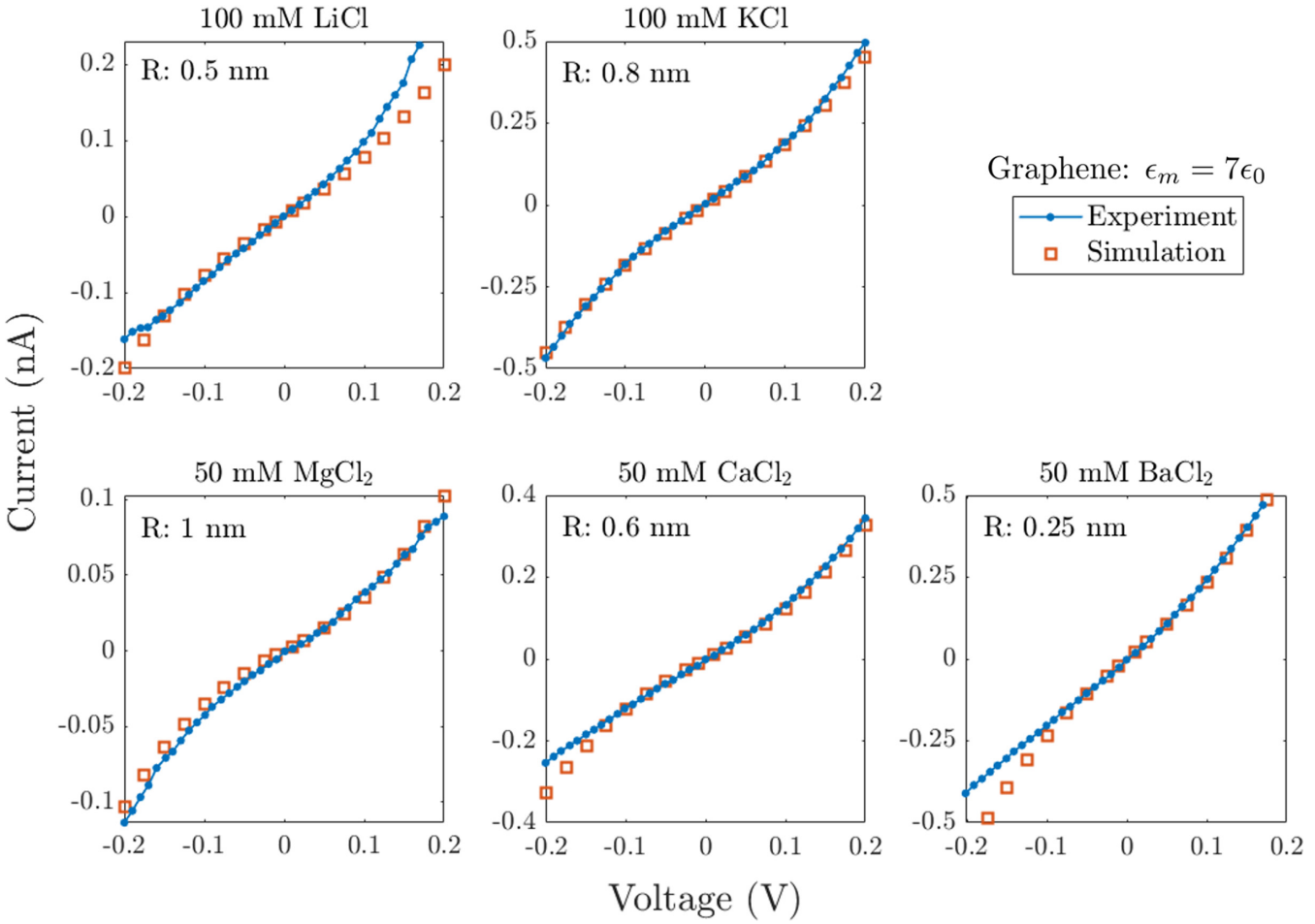

FIG. 5. Comparison of experimental (blue) and simulated (red) *I-V* data for nanoporous graphene for 100 mM LiCl, 100 mM KCl, 50 mM $MgCl_2$, 50 mM $CaCl_2$, and 50 mM $BaCl_2$ taking graphene's $\epsilon_m = 7$; with pore radii and membrane thickness in the range of 0.25–1 nm as reported by the authors.

C. Approximations

A critical output of our study is to propose simplified formulas that characterize the induced charge phenomenon based on the membrane, pore, and electrolyte parameters. Mathematically, generating simple formulas is not a straightforward task, since the induced charge profiles are impacted by nonequilibrium transport effects near the pore. The concentration profiles themselves have a complicated effect on not only the access resistance to the pore from the bulk solution, but also the resistance within the pore. We first present a simple scaling formula that captures the main trends, then we present a more detailed transport model that analytically captures the induced charge effect but involves the solution of implicit mathematical formulas.

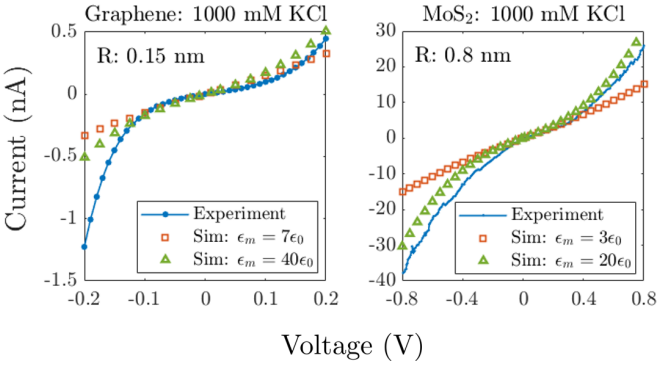

FIG. 6. Comparison of experimental (blue) and simulated (red/green) *I-V* data at high concentration (1000 mM KCl) for graphene [13] and MoS_2 [14]. We vary the value of ϵ_m in each system to show how larger values of the effective membrane permittiivty can qualitatively describe the nonlinear profile.

1. Scaling estimates

A simple scaling model can be used to obtain an initial estimate of the magnitude of the induced charge effect. The scaling model first estimates the charge density due to IC at the membrane surface assuming quasiequilibrium double layers, and subsequently use the heightened ion concentration to modify the solution conductivity.

The standard formulation for conductance across a pore considers both the entrance (access) effect and conduction within the pore. For a pore where its length is on the order of or smaller than its radius, the access resistance to the pore becomes significant. A resistance-in-series model can be used to describe the overall conductance of the pore, *G*, where the

electrical resistance is split into the access resistances on both sides of the pore and a channel resistance [14,45,46]. This approximation is widely employed in the literature and has adequately captured nanopore transport at low voltages:

$$G_A = 4\kappa_A R, \tag{5}$$

$$G_P = \frac{\kappa_P \pi R^2}{L}, \tag{6}$$

$$G = \left(2G_A^{-1} + G_P^{-1}\right)^{-1} = \kappa_A \frac{2R}{1 + \frac{2L}{\pi R}\frac{\kappa_A}{\kappa_P}}, \tag{7}$$

where κ is the electrical conductivity of the solution, with subscripts A and P referring to the access and channel, respectively. Equation (7) suggests that conductance and thus current should increase with larger pores and thinner membranes. For electrolytes,the local electrical conductivity depends on the local ion concentration and is given by

$$\kappa(c_i) = \frac{F^2}{R_g T}\sum_i z_i^2 D_i c_i, \tag{8}$$

where F is Faraday's constant, R_g is the ideal gas constant, T is the temperature, and z_i, D_i, and c_i are the valence, diffusivity, and concentration of ion i, respectively.

The conductance without IC effect, i.e., the bulk conductance G_0, can then be estimated using Eqs. (7) and (8) assuming $\kappa_A = \kappa_P = \kappa(c_{i0}) = \kappa_B$, where c_{i0} is the bulk concentration of each ion i:

$$G_0 = \kappa_B \frac{2R}{1 + \frac{2L}{\pi R}}. \tag{9}$$

G_0 is independent of V, leading to a linear I-V relationship $I = G_0 V$.

For higher applied voltages across a polarizable membrane or even a weakly polarizable membrane, the magnitude of the excess charge induced in the solution adjacent to the membrane becomes more significant. A first approximation of this induced excess charge per unit area, σ_{approx}, can be obtained using a standard capacitor-in-series (parallel plate) model that assumes low voltage drops in the Debye layer, where the overall capacitance per unit area is approximated by $C_{\text{tot}} = (2C_w^{-1} + C_m^{-1})^{-1}$:

$$\sigma_{\text{approx}} = C_{\text{tot}} V \approx \frac{\epsilon_m}{L}(1 + 2\alpha)^{-1} V, \tag{10}$$

where α is a ratio of the membrane capacitance to the Debye capacitance:

$$\alpha = \frac{\lambda_D}{L}\frac{\epsilon_m}{\epsilon_w}. \tag{11}$$

As such, α importantly describes the effective polarizability of the membrane and the relative voltage drop across the membrane and the electrolyte domains. Here, λ_D is the Debye length:

$$\lambda_D = \sqrt{\frac{\epsilon_w R_g T}{2c_0 F^2}}, \tag{12}$$

given for a 1:1 salt solution. The induced excess charge per unit area is then divided by a length scale ℓ_{layer} over which the excess ions reside and Faraday's constant to yield a per volume excess ion density expression:

$$c_{\text{IC,approx}} = \frac{\sigma_{\text{approx}}}{F\,\ell_{\text{layer}}}. \tag{13}$$

Putting the expressions together, we have the adjusted conductivity (assuming 1:1 salt with equal diffusivity D) due to induced charge as

$$\kappa_{\text{IC,approx}} \approx \frac{2F^2}{R_g T} D(c_0 + c_{\text{IC,approx}}) \tag{14}$$

which would affect both the access and pore conductance. For high V, we expect $c_{\text{IC,approx}} \gg c_0$, such that

$$I \sim G_{\text{IC}} V \sim \frac{\sigma_{\text{approx}}}{\ell_{\text{layer}}} V \sim \frac{V^2}{\ell_{\text{layer}}} \tag{15}$$

yielding a parabolic $I \sim V^2$ relationship if ℓ_{layer} is independent of V.

For the thin and small pore channel in the system, ℓ_{layer} would likely be a function of the pore geometry and the thickness of the diffuse layer from a charged surface, i.e., the Gouy-Chapman length:

$$\ell_{\text{GC}} = \frac{2\epsilon_w R_g T}{F\sigma_{\text{approx}}}. \tag{16}$$

ℓ_{GC} is defined as the distance where the interaction between an ion and the membrane surface charge σ becomes on the order of the thermal energy. Note that this approximation is valid only for low salt concentrations or highly charged surfaces [47].

If we approximate $\ell_{\text{layer}} \approx \ell_{\text{GC}}$, we have $I \sim V^3$. In this limit, the excess concentration due to induced charge can be approximated as

$$\frac{c_{\text{IC,approx}}}{c_0} \sim \frac{\alpha^2}{(1 + 2\alpha)^2}\frac{V^2}{{V_{\text{th}}}^2}, \tag{17}$$

where $V_{\text{th}} = R_g T/F = 0.026$ V is the thermal voltage. Note that this scaling model, though capturing the induced charge effect, is just a crude approximation without details of the concentration and potential profiles that depend on the problem geometry and the exact interactions between the ions and the pore in the presence of the electric field.

Figure 7(a) plots the full set of simulated currents (as specified in Table I) divided by G_0 against voltage. At low applied voltage (<0.05 V), the simulated results fall on the 1:1 line, where the linear Ohm's law holds. However, as the applied voltage becomes greater than the thermal voltage, V_{th}, the I-V curve deviates from linearity and the induced charge effect becomes stronger. This is because the ion density becomes significantly higher near the membrane in order to neutralize the induced charge on the membrane (Fig. 3). The governing parameter α, which is the membrane to Debye capacitance ratio, is the dominant factor that determines the strength of the IC effect, with higher α corresponding to higher predicted conductance. Thus, Fig. 7(a) suggests that the induced charge phenomenon over a thin, polarizable membrane can be roughly split into four regimes (Fig. 8), governed by two parameters, V/V_{th} and α, which themselves impact the

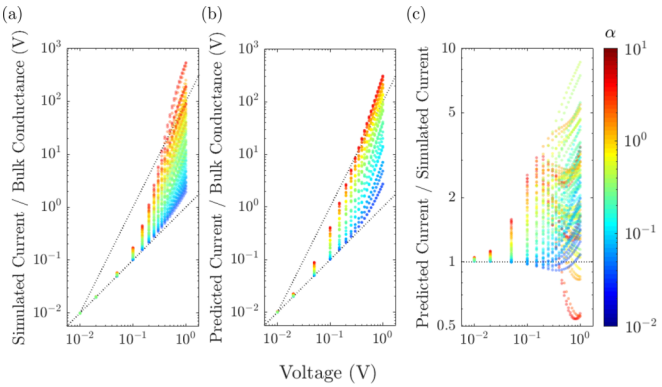

FIG. 7. (a) Simulated current scaled by bulk conductance [Eq. (9)] at various applied voltages, colored by the ratio of membrane to Debye capacitance, α. The bottom dotted line represents $x : y = 1 : 1$ where the linear I-V relationship using the bulk conductance holds, $I/G_0 = V$, i.e., no IC effect. The top dotted line has a slope of 2 and is used to guide the eye. Note that the thermal voltage is 0.026 V at 298 K. (b) Predicted current from scaling model scaled by bulk conductance, taking $\ell_{\text{layer}} = \ell_{\text{GC}}$. (c) Ratio between simulated and predicted currents in logarithmic scale.

induced excess conductivity relative to the bulk conductivity. Figure 7(b) plots the predictions by the scaling model and (c) the deviations between simulation and scaling in logarithmic scale, with an approximation for the distance to which ions responding to the induced charge extend out as $\ell_{\text{layer}} = \ell_{\text{GC}}$. The scaling model captures the IC behavior with a relatively similar spread of α values within an order of magnitude, with a bias towards overestimation. The overestimation could stem from using the externally applied voltage V to approximate the potential difference across the membrane that drives the current, which would in actuality be lower and its determination would require knowledge of the potential profile. In addition, because the scaling does not involve solving Poisson's equation, it fails to capture the exponential onset of the IC effect around V_{th}.

		Applied *vs.* Thermal Voltage	
		$V \ll \frac{k_B T}{F}$	$V \gg \frac{k_B T}{F}$
Membrane *vs.* Debye Capacitance	$\alpha > \sim 1$	Ohm's Law (linear)	large IC (nonlinear)
	$\alpha \ll 1$	Ohm's Law (linear)	small IC (near-linear)

FIG. 8. Regimes for induced charge effects for thin, polarizable membranes.

2. *Reduced model*

To complement the results of the simulations and the simple scaling argument, we propose a reduced model to analytically capture the induced charge conduction effect. In order to retain analytical tractability, the model does not describe the full extent of nonequilibrium ion concentration profiles. Even so, it provides a clear guide for the trends in the full 2D simulation data as a function of the physical properties of the electrolyte, membrane, and pore domains. Our strategy relies on (i) assuming quasiequilibrium double layers to derive implicit formulas for the effective ionic concentrations at the membrane surface and the extent of surface conduction, (ii) using the surface conductivity to estimate an effective radius of the pore and thus the access conductance, and (iii) assuming overlapping double layers within the pore to estimate the channel conductance.

In order to introduce the surface conduction via induced charge into the simplified model, we will first assume quasiequilibrium double layers at the membrane interfaces. Such an approach effectively defines the equilibrium double layer structure in the absence of the nanopore, and then considers the nanopore as a perturbation upon the equilibrium conformation to determine the nanopore conductance in the presence of induced charge. While the ionic concentration profiles in and around the pore can vary significantly from the equilibrium conformation, we expect the model to qualitatively reproduce the current voltage characteristics of the induced charge phenomenon. The analysis is restricted to a 1:1 salt with equal ionic diffusivities $D_+ = D_- = D$. We separate the contributions of induced charge first to the access resistance and then to the pore resistance.

As an initial step for the induced charge effect on access resistance, we decompose the potential into an equilibrium part, $\psi(z)$, one that forms the double layers at the membrane interfaces, and a nonequilibrium part, $\phi_v(x, y, z)$, that drives ionic currents.

$$\phi(x, y, z) = \psi(z) + \phi_v(x, y, z). \tag{18}$$

The equilibrium part of the potential, $\psi(z)$, is strictly defined at the reservoir-facing membrane interfaces, and disturbances by the presence of the pore are neglected. The equilibrium part of the potential satisfies

$$-\epsilon_w \frac{d^2\psi}{dz^2} = \rho_e, \tag{19}$$

as the derivatives in ϕ_v are assumed to be much slower varying than ψ. The accompanying boundary condition of $j_{iz} = 0$ at the membrane interface ensures that

$$c_i = c_{i0} \exp\left(-\frac{z_i \psi}{V_{\text{th}}}\right), \tag{20}$$

thus providing a Poisson-Boltzmann equation for the ionic concentrations, with boundary condition of

$$\epsilon_w \left.\frac{d\psi}{dz}\right|_w = \epsilon_m \left.\frac{d\psi}{dz}\right|_m,$$
$$\psi(z \to -\infty) = -V/2, \quad \psi(z \to \infty) = V/2, \tag{21}$$

where V is the voltage drop across the membrane. The equilibrium conformation of the double layer next to a

thin membrane as a function of voltage has been studied previously [48]. In the absence of surface charges, the Poisson-Boltzmann equation can be integrated to relate the potential drop across the membrane to the potential at the membrane interfaces at $z = 0$ and $z = L$. We define the quantity ψ_0 as $\psi_0 = \psi(z = 0) + V/2 = V/2 - \psi(z = L)$, to give the following formula:

$$\alpha^2 \frac{(V - 2\psi_0)^2}{V_{\rm th}^2} = 4\sinh^2\left(\frac{\psi_0}{2V_{\rm th}}\right), \tag{22}$$

where α, again, is the ratio of the membrane capacitance to the Debye capacitance. The above expression gives an implicit expression for the potential at the membrane interfaces far from the pore mouth, ψ_0, relative to the reservoir potentials on each side. It is the magnitude of ψ_0 that determines the extent of the induced charge at the membrane interfaces. We can apply the estimate for ψ_0 to describe the ionic concentrations in and around the pore that give the higher concentration profile there. For example, the local conductivity at the membrane interfaces, κ, can be estimated by applying Eq. (20) and assuming equal ionic diffusion coefficients to give $\kappa = \kappa_B(c_+ + c_-)/(2c_0) = \kappa_B \cosh(\psi_0/V_{\rm th})$, which means that the local conductivity increases near the membrane interfaces. In solving the nonlinear equation (22), we choose the root where $0 \leqslant |\psi_0| \leqslant |V|/2$ and where ψ_0 has the same sign as V. At small applied potentials, the implicit formula can be expanded to give

$$\psi_0 = \frac{\alpha}{(1 + 2\alpha)} V, \tag{23}$$

consistent with the simple scaling argument in Eq. (10) for the induced charge. We now apply the implicit formula in Eq. (22) in the nonlinear regime to characterize transport. First, we use ψ_0 to estimate the surface conduction and effective radius to access the pore mouth to arrive at G_A. Then, we apply the definition of ψ_0 to describe the conductivity within the pore to estimate the channel conductance, G_P.

In the absence of bulk concentration gradients, the current density reduces to

$$\mathbf{J} = \sum_i z_i F J_i = -\kappa(c_i)\nabla\phi_v, \tag{24}$$

where the conductivity depends on the local ionic concentration, c_i. Here, the ionic concentration is set by the equilibrium component of the electrostatic potential, ψ, but the current is driven by gradients in the nonequilibrium component, ϕ_v. Far from the membrane, the ion concentrations equal their bulk values, and the current density and charge conservation become

$$\mathbf{J}_\infty = -\kappa_B \nabla\phi_v, \quad \nabla^2\phi_v = 0, \tag{25}$$

where κ_B is the bulk conductivity of the solution. Near the interfaces, the local conductivity is higher owing to the accumulation of ionic charges. Along the membrane surfaces, the excess current through the double layers can be derived by integrating over the double layer region into the bulk [49]:

$$\mathbf{J}_s = \int_0^\infty \mathbf{J} - \mathbf{J}_\infty dz = -4\lambda_D \kappa_B \sinh^2\left(\frac{\psi_0}{4V_{\rm th}}\right)\nabla_s\phi_v, \tag{26}$$

where ∇_s is the surface gradient. The surface current, $\mathbf{J}_s$, has units of current per length, and allows us to neglect the precise details of the electrostatic potential profile within the double layers and to collapse all the current attributable to the double layers to the membrane surface. In terms of the Dukhin length, $\ell_{\rm Du} = 4\lambda_D \sinh^2(\psi_0/4V_{\rm th})$, defined as the surface conductance divided by the bulk conductance, we can rewrite the expression for the surface current as

$$\mathbf{J}_s = -\ell_{Du}\kappa_B \nabla_s\phi_v. \tag{27}$$

Owing to the higher conductivity in the double layers, the surface conductance can "short circuit" a region of radius $R_{\rm eff}$ towards the pore mouth, such that the system with induced charge acts as a pore of effective radius $R_{\rm eff}$ instead of R. The region on the membrane surface within a radius $R_{\rm eff}$ can be thought of as an expanded pore opening without the IC effect that would have the same access conductance as the actual pore opening in the presence of the IC effect. If the variable ϕ_v in the circular region enclosed by the effective radius $R_{\rm eff}$ is approximately constant, then the far field profile for ϕ_v that satisfies $\nabla^2\phi_v = 0$ is given by

$$\phi_v \approx \frac{2\Delta V R_{\rm eff}}{\pi r}, \tag{28}$$

where ΔV is the potential drop between the pore mouth and the bulk that drives ionic currents, and r is the spherical radial coordinate centered at the pore opening [50].

The resulting access conductance is the bulk conduction towards a pore of radius $R_{\rm eff}$, consistent with Eq. (25):

$$G_A = 4\kappa_B R_{\rm eff}. \tag{29}$$

The approximate scale of $R_{\rm eff}$ is set by the balance between the surface conductance in an annular region around the pore and the access resistance from the bulk. The conductance through an annular region on the surface between $r = R$ and $r = R_{\rm eff}$ is determined by solving charge conservation in cylindrical coordinates along the surface using Eq. (27):

$$-\kappa_B \ell_{\rm Du} \frac{1}{r}\frac{d}{dr}\left(r\frac{d\phi_v}{dr}\right) = 0 \tag{30}$$

with the resulting conductance of the annular region, $G_{\rm annulus}$, given by

$$G_{\rm annulus} = \frac{2\pi \ell_{\rm Du}\kappa_B}{\ln(R_{\rm eff}/R)}. \tag{31}$$

Here, to estimate $R_{\rm eff}$, we assume the conductance to access the pore mouth must be comparable to conductance in the annular region, in order for the pore mouth ($r < R$) and annular region ($R < r < R_{\rm eff}$) to roughly have an equal value of ϕ_v. The mathematical approximation is therefore

$$G_{\rm annulus} \approx G_P \rightarrow \frac{2\pi \ell_{\rm Du}\kappa_B}{\ln(R_{\rm eff}/R)} \approx 4\kappa_B R_{\rm eff}. \tag{32}$$

The above expression allows for the approximation of $R_{\rm eff}$ in terms of the product logarithmic function, $W(\cdot)$:

$$R_{\rm eff} = R\exp\left[W\left(\frac{\pi \ell_{\rm Du}}{2R}\right)\right]. \tag{33}$$

The estimated value of $R_{\rm eff}$ above can be considered as an upper bound because the true induced charge near the pore

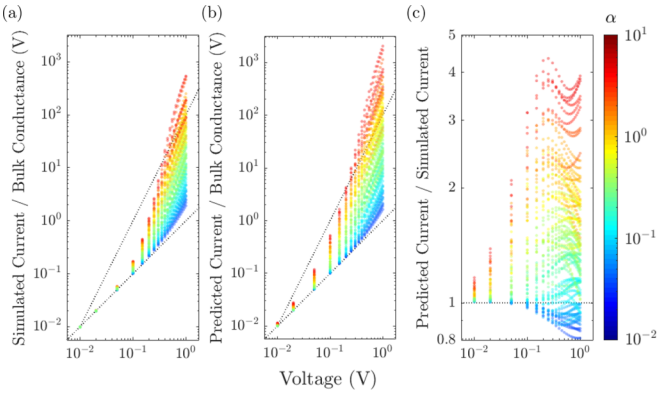

FIG. 9. (a) Simulated current scaled by bulk conductance [Eq. (9)]. The bottom dotted line represents $x{:}y = 1{:}1$ where the linear I-V relationship using the bulk conductance holds, $I/G_0 = V$, i.e., no IC effect. The top dotted line has a slope of 2 and is used to guide the eye—the IC effect approaches near parabolic I-V relationship at high voltages. (b) Predicted current from reduced model theory scaled by bulk conductance, derived by substituting Eqs. (29) and (35) into Eq. (7). (c) Ratio between simulated and predicted currents.

is less than the induced charge far from the pore owing to deformation of the double layer structure by the ionic currents. At low applied voltage, the effective radius relative to the actual radius is

$$\frac{R_{\text{eff}}}{R} \approx 1 + \frac{\pi}{8}\left(\frac{\lambda_D}{R}\right)\frac{\alpha^2}{(1+2\alpha)^2}\frac{V^2}{{V_{\text{th}}}^2}, \tag{34}$$

consistent with the scaling in Eq. (17), but including an additional dependence on the ratio of the Debye length and the pore radius.

Inside the pore, in the limit of strongly overlapping double layers of our analysis, the concentration should be uniform. Here, the expressions for surface conduction for nonoverlapping double layers in Eqs. (26) and (27) cannot be employed. Instead, we assume a conductivity within the pore set by the induced surface potential on each membrane interface, $\kappa_P = \kappa_B \cosh(\psi_0/V_{\text{th}})$, by summing over all the ionic species contribution to the conductivity. This assumption gives a channel conductance of

$$G_P = \frac{\pi R^2 \kappa_B}{L}\cosh\left(\frac{\psi_0}{V_{\text{th}}}\right). \tag{35}$$

At low applied voltage, the conductivity within the pore scales as

$$\frac{\kappa_P}{\kappa_B} = 1 + \frac{\alpha^2}{2(1+2\alpha)^2}\frac{V^2}{{V_{\text{th}}}^2}, \tag{36}$$

again consistent with the simple scaling argument in Eq. (17). While large errors are expected within the pore domain, the above expression gives an estimate for the conductance increase as the screening charges are swept into the pore domain from the membrane surfaces.

The overall conductance is again a result of the access and pore resistances in series, plugging in Eqs. (29) and (35) into Eq. (7). The results of these approximations are plotted in Fig. 9. In general, the reduced model overpredicts the current through the pore at a given voltage, similar to the simpler scaling arguments in the previous section. The overprediction is due to the variation of the actual surface potential or Dukhin length near the pore mouth and complicated entrance effects. Even so, the reduced model captures the key qualitative features of the fully numerical simulations with much simpler analytical formulas and more information about the pore and membrane domains.

IV. CONCLUSION

In this paper, we have demonstrated that IC phenomena could explain the nonlinear I-V curves observed in numerous experiments of ion transport across subnano- and nanopores across atomically thin membranes such as graphene and MoS_2. Approximate formulas based on simple scaling arguments and an analytical transport model were developed to predict current-voltage relationships, which qualitatively match with numerical simulations. Based on our theoretical analysis, the key parameters in determining the extent of IC effects are the membrane capacitance and the ionic concentration. Higher membrane capacitance (from thinner or more polarizable membranes) translates to more induced charge at the membrane interfaces. At lower ionic concentration, the induced charge effect dominates over the bulk conductivity near the pore mouth. As the applied voltage across an ultrathin membrane increases, more charge is induced at the membrane interfaces leading to strong nonlinearities at high voltage.

Future work could consider the presence of additional effects within the continuum model, such as fixed surface charge, reservoirs at asymmetric ionic concentrations, ion crowding, dehydration, and asymmetric membrane structures, at high voltage and salt concentrations. Critically, the capacitance in Stern layers and saturation of ionic concentrations in the crowded regime could influence the effective membrane capacitance and thus the current voltage relation. More sophisticated molecular dynamics simulations could incorporate the charge induced by individual ions [51,52] and the role of dehydration and ion correlations by explicitly representing the discrete solvent molecules and ions. Furthermore, the detailed electronic properties of the membrane could also be important in determining the capacitance of the membrane and thus the magnitude of induced charge. While we have treated the membrane as an ideal dielectric, the quantum capacitance of graphene is significant [53,54]. Doping of the membrane domain by specific molecules might change the effective capacitance and the current-voltage characteristics [55]. As more specific details are added to the induced charge models, more complex current-voltage relationships might be related to the induced charge phenomenon.

ACKNOWLEDGMENTS

J.P.d.S. was supported as part of the Center for Enhanced Nanofluidic Transport, and Energy Frontier Research Center funded by the U.S. Department of Energy, Office of Science, Basic Energy Sciences under Award No. DE-SC0019112, and from the National Science Foundation Graduate Research Fellowship under Award No. 1122374. C.M.C. acknowledges

support by the National Science Foundation Graduate Research Fellowship under Grant No. 1745302, the Croucher Foundation, and the MIT Abdul Latif Jameel Water and Food Systems Lab.

[1] L. Wang, M. S. Boutilier, P. R. Kidambi, D. Jang, N. G. Hadjiconstantinou, and R. Karnik, Nat. Nanotechnol. **12**, 509 (2017).

[2] S. P. Koenig, L. Wang, J. Pellegrino, and J. Bunch, Nat. Nanotechnol. **7**, 728 (2012).

[3] M. S. Boutilier, D. Jang, J.-C. Idrobo, P. R. Kidambi, N. G. Hadjiconstantinou, and R. Karnik, ACS Nano **11**, 5726 (2017).

[4] S. C. O'Hern, M. S. Boutilier, J.-C. Idrobo, Y. Song, J. Kong, T. Laoui, M. Atieh, and R. Karnik, Nano Lett. **14**, 1234 (2014).

[5] J. Zhao, G. He, S. Huang, L. Villalobos, M. Dakhchoune, H. Bassas, and K. Agrawal, Sci. Adv. **5**, eaav1851 (2019).

[6] L. Wang, C. M. Williams, M. S. Boutilier, P. R. Kidambi, and R. Karnik, Nano Lett. **17**, 3081 (2017).

[7] P. R. Kidambi, D. Jang, J.-C. Idrobo, M. S. Boutilier, L. Wang, J. Kong, and R. Karnik, Adv. Mater. **29**, 1700277 (2017).

[8] C. Sun, B. Wen, and B. Bai, Sci. Bull. **60**, 1807 (2015).

[9] D. Cohen-Tanugi and J. C. Grossman, Nano Lett. **12**, 3602 (2012).

[10] S. Garaj, S. Liu, J. A. Golovchenko, and D. Branton, Proc. Natl. Acad. Sci. USA **110**, 12192 (2013).

[11] Z. Yuan, J. D. Benck, Y. Eatmon, D. Blankschtein, and M. S. Strano, Nano Lett. **18**, 5057 (2018).

[12] J. Feng, M. Graf, K. Liu, D. Ovchinnikov, D. Dumcenco, M. Heiranian, V. Nandigana, N. R. Aluru, A. Kis, and A. Radenovic, Nature (London) **536**, 197 (2016).

[13] T. Jain, B. C. Rasera, R. J. S. Guerrero, M. S. Boutilier, S. C. O'hern, J.-C. Idrobo, and R. Karnik, Nat. Nanotechnol. **10**, 1053 (2015).

[14] J. P. Thiruraman, K. Fujisawa, G. Danda, P. M. Das, T. Zhang, A. Bolotsky, N. Perea-López, A. Nicolaï, P. Senet, M. Terrones *et al.*, Nano Lett. **18**, 1651 (2018).

[15] R. C. Rollings, A. T. Kuan, and J. A. Golovchenko, Nat. Commun. **7**, 11408 (2016).

[16] L. Cantley, J. L. Swett, D. Lloyd, D. A. Cullen, K. Zhou, P. V. Bedworth, S. Heise, A. J. Rondinone, Z. Xu, S. Sinton, and J. S. Bunch, Nanoscale **11**, 9856 (2019).

[17] M. Z. Bazant and T. M. Squires, Phys. Rev. Lett. **92**, 066101 (2004).

[18] T. M. Squires and S. R. Quake, Rev. Mod. Phys. **77**, 977 (2005).

[19] S. M. Davidson, M. B. Andersen, and A. Mani, Phys. Rev. Lett. **112**, 128302 (2014).

[20] H. Feng, Y. Huang, T. N. Wong, and F. Duan, Soft Matter **13**, 4864 (2017).

[21] G. Yossifon, I. Frankel, and T. Miloh, Phys. Fluids **19**, 068105 (2007).

[22] S. Gangwal, O. J. Cayre, M. Z. Bazant, and O. D. Velev, Phys. Rev. Lett. **100**, 058302 (2008).

[23] D. Saintillan, E. Darve, and E. S. Shaqfeh, J. Fluid Mech. **563**, 223 (2006).

[24] T. M. Squires, *Fluids, Colloids and Soft Materials: An Introduction to Soft Matter Physics* (Wiley, New York, 2016), p. 59.

[25] M. Z. Bazant and T. M. Squires, Curr. Opin. Colloid Interface Sci. **15**, 203 (2010).

[26] T. M. Squires, Lab Chip **9**, 2477 (2009).

[27] S. Park and G. Yossifon, Phys. Rev. E **93**, 062614 (2016).

[28] H.-C. Chang, G. Yossifon, and E. A. Demekhin, Annu. Rev. Fluid Mech. **44**, 401 (2012).

[29] G. Yossifon, I. Frankel, and T. Miloh, Phys. Fluids **18**, 117108 (2006).

[30] S. K. Thamida and H.-C. Chang, Phys. Fluids **14**, 4315 (2002).

[31] M. Mao, S. Ghosal, and G. Hu, Nanotechnology **24**, 245202 (2013).

[32] F. Ziebert, M. Z. Bazant, and D. Lacoste, Phys. Rev. E **81**, 031912 (2010).

[33] D. Lacoste, G. Menon, M. Bazant, and J. Joanny, Eur. Phys. J. E **28**, 243 (2009).

[34] Y. Yao, C. Wen, N. H. Pham, and S.-L. Zhang, Langmuir **36**, 8874 (2020).

[35] P. Rickhaus, M.-H. Liu, M. Kurpas, A. Kurzmann, Y. Lee, H. Overweg, M. Eich, R. Pisoni, T. Taniguchi, K. Watanabe *et al.*, Sci. Adv. **6**, eaay8409 (2020).

[36] J. Fang, W. G. Vandenberghe, and M. V. Fischetti, Phys. Rev. B **94**, 045318 (2016).

[37] B. Li, T. Saito, and N. Okamoto, in *2018 International Conference on Electronics Packaging and iMAPS All Asia Conference (ICEP-IAAC)* (IEEE, New York, 2018), pp. 539–542.

[38] M. Belete, S. Kataria, U. Koch, M. Kruth, C. Engelhard, J. Mayer, O. Engstrom, and M. C. Lemme, ACS Appl. Nano Mater. **1**, 6197 (2018).

[39] M. Ghosh, K. F. Jorissen, J. A. Wood, and R. G. Lammertink, J. Phys. Chem. Lett. **9**, 6339 (2018).

[40] M. Zhang, K. Guan, Y. Ji, G. Liu, W. Jin, and N. Xu, Nat. Commun. **10**, 1253 (2019).

[41] C. Lee, L. Joly, A. Siria, A.-L. Biance, R. Fulcrand, and L. Bocquet, Nano Lett. **12**, 4037 (2012).

[42] R. M. Wyss, T. Tian, K. Yazda, H. G. Park, and C.-J. Shih, Nano Lett. **19**, 6400 (2019).

[43] B. Hille, *Ion Channels of Excitable Membranes* (Sinauer, Sunderland, MA, 2001).

[44] M. Z. Bazant, M. S. Kilic, B. D. Storey, and A. Ajdari, Adv. Colloid Interface Sci. **152**, 48 (2009).

[45] S. Sahu and M. Zwolak, Phys. Chem. Chem. Phys. **20**, 4646 (2018).

[46] J. E. Hall, J. Gen. Physiol. **66**, 531 (1975).

[47] L. Bocquet and E. Charlaix, Chem. Soc. Rev. **39**, 1073 (2010).

[48] S. Genet, R. Costalat, and J. Burger, Acta Biotheor. **48**, 273 (2000).

[49] J. Lyklema, *Solid-Liquid Interfaces*, Fundamentals of Interface and Colloid Science, Vol. II (Elsevier, New York, 1995).

[50] J. Newman, J. Electrochem. Soc. **113**, 501 (1966).

[51] R. P. Misra and D. Blankschtein, J. Phys. Chem. C **121**, 28166 (2017).

[52] R. P. Misra and D. Blankschtein, Langmuir **37**, 722 (2021).

[53] T. Fang, A. Konar, H. Xing, and D. Jena, Appl. Phys. Lett. **91**, 092109 (2007).

[54] Z. Mišković and N. Upadhyaya, Nanoscale Res. Lett. **5**, 505 (2010).

[55] L. L. Zhang, X. Zhao, H. Ji, M. D. Stoller, L. Lai, S. Murali, S. Mcdonnell, B. Cleveger, R. M. Wallace, and R. S. Ruoff, Energy Environ. Sci. **5**, 9618 (2012).